

Multiscale analysis of long-term mechanical and durability behaviour of two alkali-activated slag-based types of concrete

Bezemer, H. J.; Awasthy, N.; Luković, M.

DOI

[10.1016/j.conbuildmat.2023.133507](https://doi.org/10.1016/j.conbuildmat.2023.133507)

Publication date

2023

Document Version

Final published version

Published in

Construction and Building Materials

Citation (APA)

Bezemer, H. J., Awasthy, N., & Luković, M. (2023). Multiscale analysis of long-term mechanical and durability behaviour of two alkali-activated slag-based types of concrete. *Construction and Building Materials*, 407, Article 133507. <https://doi.org/10.1016/j.conbuildmat.2023.133507>

Important note

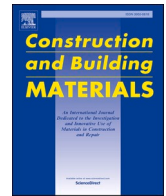
To cite this publication, please use the final published version (if applicable).
Please check the document version above.

Copyright

Other than for strictly personal use, it is not permitted to download, forward or distribute the text or part of it, without the consent of the author(s) and/or copyright holder(s), unless the work is under an open content license such as Creative Commons.

Takedown policy

Please contact us and provide details if you believe this document breaches copyrights.
We will remove access to the work immediately and investigate your claim.



Multiscale analysis of long-term mechanical and durability behaviour of two alkali-activated slag-based types of concrete

H.J. Bezemer^{*}, N. Awasthy, M. Luković

Delft University of Technology, Stevinweg 1, Delft 2628CN, the Netherlands

ARTICLE INFO

Keywords:

Alkali activated concrete
Long-term mechanical properties
Reinforced alkali activated concrete beams
Time-dependent crack-widths
Development of bending stiffness

ABSTRACT

Although alkali activated concretes (AACs) are promising for reducing the carbon emissions of concrete, in order to enable their wide application it is vital to understand their long-term behaviour. Herein, we report the development of mechanical properties of a ground granulated blast furnace slag (GGBFS)-based AAC and a binary fly ash (FA) /GGBFS-based AAC exposed to 55% relative humidity and 20 °C up to the age of 5 years. For comparison, two ordinary Portland cement (OPC) concretes were monitored for 3.5 years. For the GGBFS-based AAC, after an initial decrease within the first 6 months the elastic compressive modulus stabilized, while its tensile splitting strength continued to decrease for the tested period of 5 years. The binary AAC showed a continuous decrease in its tensile splitting strength for 5 years and a reduction in its compressive strength after 2 years. No decreases in mechanical properties were observed in OPC-based concretes. To reveal underlying mechanisms, additional analyses were performed. Permanent degradation was observed in both AACs; the binary AAC mainly suffered from carbonation, and the GGBFS-based AAC showed microcracking. These cracks were probably caused by drying shrinkage and drying-induced chemical changes. Based on the measured mechanical properties of AAC, crack widths and stiffness of reinforced AAC beams under bending were analytically evaluated and compared to experiments. Decreases in bending stiffness and increases in crack width were observed for reinforced AAC beams tested at later ages. A bimodular approach is proposed to predict the reduction of bending stiffness in the studied AACs over time. These findings are relevant to understand serviceability limit states of reinforced AACs.

1. Introduction

Concrete is the second most widely used material in the world [1]. Although concrete has enabled prosperity, due to its widespread usage, the concrete industry is responsible for 5–8% of the anthropogenic carbon footprint [2–4]. To limit global warming to 2 °C by 2100, current CO₂-emissions from cement production should be reduced with 24% by 2050 [5]. This is challenging as current global cement production is expected to grow 12–23% by 2050 [5]. One way to reduce the CO₂-emissions of concrete is to replace ordinary Portland cement (OPC) based binders with alkali activated binders [5,6]. Ground Granulated Blast Furnace Slag (GGBFS) and coal Fly Ash (FA) are often used for alkali activation, due to their wide availability as industrial by-products.

Alkali activated concretes (AACs) are not yet widely applied in practise due to a lack of design codes and guidelines. It is unclear whether design codes for Ordinary Portland Cement-based concretes (OPCCs) are applicable for AACs, since the empirical relations in these

codes are mainly based on the 28th day compressive strength. For OPCCs, it is conservative to use the 28th day strength: beyond 28 days, OPCCs show an increase in the mechanical properties [7–13] due to ongoing cement hydration [14]. On the contrary, alkali activation of GGBFS is a rapid polymerization process which could lead to stagnation of the strength development after 28 days [15]. Alkali activation of FA under ambient temperatures is a slower reaction and, therefore, a binary FA/GGBFS precursor is sometimes adopted to enhance the strength gain beyond 28 days [15]. Nevertheless, decreasing mechanical properties have been observed for GGBFS-based and binary FA/GGBFS-based AACs over time [16–23]. For binary FA/GGBFS-based AACs, these decreases may be related to carbonation, which causes decalcification of the microstructure [24,25]. This decalcification leads to carbonation shrinkage, which could lead to micro cracking and reduction of strength and stiffness [24,25]. GGBFS-based AACs are less susceptible to carbonation due to their dense pore structures, high Ca/Si ratios and limited consumption of Na⁺-ions from their pore solutions [25].

^{*} Corresponding author.

E-mail address: H.J.Bezemer@tudelft.nl (H.J. Bezemer).

<https://doi.org/10.1016/j.conbuildmat.2023.133507>

Received 13 April 2023; Received in revised form 25 August 2023; Accepted 21 September 2023

Available online 28 September 2023

0950-0618/© 2023 The Author(s). Published by Elsevier Ltd. This is an open access article under the CC BY license (<http://creativecommons.org/licenses/by/4.0/>).

Decreases in their mechanical properties may be related to (1) significant drying shrinkage compared to OPCCs [18,19,21,26–28] and (2) chemical changes upon drying [29]. However, published studies are difficult to compare since different mix designs, curing methods, and exposure conditions have been used. Furthermore, in our previous study no microstructural changes were observed at the age of 2 years [23]. Based on this, we hypothesize that the observed decreases in binary FA/GGBFS-based AACs and GGBFS-based AACs could be temporary.

For structural application of AACs, it is important to understand the long term material behaviour and study the structural behaviour of AACs over time. However, most studies focused on performing structural tests at 28 days. At the age of 28 days, reinforced FA-based AACs show similar cracking loads [30,31], tension stiffening response [30], cracking patterns [30–33] and concrete-rebar bond [34] compared to reinforced OPCCs. On the other hand, GGBFS-based AACs could show larger crack widths and crack spacings than OPCCs at the age of 28 days [35,36]. These larger crack widths might be related to a lower tension stiffening effect of reinforced GGBFS-based AAC beams compared to OPCCs at the age of 28 days [35]. Although our previous study [23] investigated reinforced GGBFS-based and FA/GGBFS-based AAC beams tested at different ages, we did not analyse the crack widths in detail. Therefore, the impact of the development of mechanical properties of GGBFS-based and FA/GGBFS-based AACs on the development of crack widths over time is unclear. In addition, the development of bending stiffness of AACs is important for the prediction of long-term deflections and the serviceability design of structural concrete [18]. Although lower bending stiffnesses compared to OPCC [36] were already observed for GGBFS-based AACs at the age of 28 days, the effect of decreasing elastic compressive modulus on the development of the bending stiffness has not been addressed so far. Hence, the effect of the development of the elastic modulus on the bending stiffness of reinforced AACs should be studied.

The aim of this study is to understand the long-term development of mechanical properties of two AACs and evaluate the effect of decreasing mechanical properties on the development of crack widths and bending stiffnesses of reinforced GGBFS-based and FA/GGBFS-based AACs over time. Mechanical properties of two AACs, different by their GGBFS-content, were monitored for 5 years to test if previously observed decreases are temporary. A normal and a high strength OPC-based concrete are monitored for 3.5 years for comparison. Three additional analyses are performed to explain the decreases of long-term mechanical properties and reveal the underlying mechanisms: (1) non-linearity of stress–strain curves in compression, (2) carbonation depth and (3) microscopic images of epoxy-impregnated samples. With the insights from these additional analyses, the development of crack widths and bending stiffness for reinforced concrete beams are evaluated and compared to analytical predictions at different ages. A bi-modular approach is proposed to predict the development of bending stiffness of reinforced beams over time.

2. Materials and methods

2.1. Mix proportions and specimen preparation

Two AAC mixtures with different types of precursors are studied: (1) a GGBFS precursor (mixture denoted as S100) and (2) a binary precursor containing 50% per weight (wt%) of GGBFS and 50 wt% of FA (mixture denoted as S50). The specific gravities of GGBFS and FA are 2890 kg/m³

and 2440 kg/m³, respectively. The chemical compositions of the used GGBFS and FA are shown in Table 1. Both AACs are activated by an alkaline solution made by mixing a sodium hydroxide solution (4 M) with a sodium silicate solution (27.5 wt% SiO₂, 8.25 wt% Na₂O and 64.25 wt% H₂O) in a 1:1 wt proportion. The resulting solution has a Na₂O concentration of 4.8 wt% and a silica modulus (SiO₂/Na₂O) of 1.45. The alkaline solution is prepared 24 h prior to casting.

For comparison, three OPCCs are included in the study (Table 2): (1) a normal strength concrete made of CEM I 42.5 N (mixture denoted as NSC-42.5) and with a similar elastic modulus as S100, (2) a normal strength concrete made of CEM I 52.5 N (mixture denoted as NSC-52.5) and with a similar elastic modulus as S100, and (3) a high strength concrete (mixture denoted as HSC) with a similar compressive strength as S50. MasterGlenium 51 (35% concentrated) superplasticizer is used to improve the workability of NSC-52.5 (Table 2). NSC-52.5 is used in structural tests for comparison to the AACs.

After casting, the samples are vibrated for approximately 20 s, followed by sealed curing for 24 h. Next, the samples are demoulded and placed inside a fog room under 95% relative humidity (RH) and 20 °C. After a 28-day curing period, all samples are exposed to controlled laboratory conditions (55% RH, 20 °C) until testing.

2.2. Material behaviour

Due to a lack of standards for AACs, standards developed for conventional OPC concretes are followed for testing the properties of AACs. The compressive strength, tensile splitting strength, and elastic compressive modulus of OPCCs and AACs are investigated for a duration of 3.5 and 5 years, respectively. These properties are used further in analytical predictions of the structural behaviour.

The compressive strength is determined on 100 mm cubes loaded with a constant rate of 0.65 MPa/s. The test is performed according to EN 12390-3 [38]. For the tensile splitting strength, 100 mm cubes are tested with a constant loading rate of 1.1 kN/s, according to EN 12390-6 [39]. To determine the elastic compressive modulus, 100 × 100 × 400 mm³ prisms are tested with a loading rate of 0.65 MPa/s. Following method B of EN 12390-13 [40], the elastic compressive modulus is determined from the last loading cycle from 10% up to 33% of the mean compressive prism strength ($f_{cm,prism}$). The compressive prism strength is estimated from the cube strength, assuming the ratio of 0.85 as reported for conventional concrete [41–43]. This assumption should be verified in future studies. Three specimens were used in each test. The measured elastic compressive modulus might slightly differ from those reported in

Table 2
Mix proportions for the studied AACs and OPCCs.

	S100	S50	NSC-42.5	HSC	NSC-52.5
Ingredient	(kg/m ³)	(kg/m ³)	(kg/m ³)	(kg/m ³)	(kg/m ³)
GGBFS	400	200	0	0	0
FA	0	200	0	0	0
CEM I 42.5 N	0	0	260	0	0
CEM I 52.5 R	0	0	0	366.7	260
Sand (0–4 mm)	784	784	847.4	841.7	847.4
Gravel (4–8 mm)	435.5	435.5	394.2	373.3	394.2
Gravel (8–16 mm)	522.5	522.5	729.2	653.3	729.2
Activating solution	212	212	156	166.7	156
Superplasticizer	–	–	–	–	0.26
l/b-ratio	0.53	0.53	0.6	0.45	0.6

Table 1
Chemical composition of used precursors, determined by X-ray fluorescence results by Nedeljković et al. [37].

[%]	SiO ₂	Al ₂ O ₃	CaO	MgO	Fe ₂ O ₃	S	Na ₂ O	K ₂ O	TiO	P ₂ O ₅	LOI
GGBFS	35.5	13.5	39.8	8.0	0.6	1.0	0.4	0.5	1.0	0.0	–1.3
FA	56.8	23.8	4.8	1.5	7.2	0.3	0.8	1.6	1.2	0.5	1.2
CEM I	19.6	4.8	62.2	1.8	3.0	1.4	0.4	0.6	0.3	0.2	2.8

our earlier study [23], as the average elastic modulus was determined over all three load cycles, instead of only the last load cycle.

Internal structures of the studied concretes are assessed for potential damage to understand the cause of decreasing mechanical properties of AACs. The presence of internal damage can be inferred from the non-linearity of the compressive stress–strain curve [44]. Similar as in EN 12390-13 [40], this non-linearity is quantified by the coefficient of variation from two elastic moduli: (1) determined from 10% to 20% of the mean compressive prism strength ($f_{cm,prism}$) and (2) determined from 10% to 33% $f_{cm,prism}$. Both moduli are obtained from the third loading cycle. In addition, the carbonation depth is determined at the final testing ages (3.5 years and 5 years for OPCC and AACs, respectively) with phenolphthalein following the procedure of EN 13295 [45]. Lastly, microscopic images from epoxy impregnated samples with a size of $45 \times 45 \times 10 \text{ mm}^3$ are analysed to investigate the presence of (micro) cracks. These samples are sawn out of 100 mm cubes using a water-cooled saw. After sawing, the samples are dried at room temperature and vacuum impregnated with fluorescent epoxy. Next, the top layer is removed by grinding. An optical UV-light microscope is used for imaging of the samples. To improve the visibility of the impregnated epoxy, the images are post-processed with ImageJ [46] as follows: (1) the contrast is enhanced to 0.35% pixel saturation, (2) the format is converted to 8-bit by splitting the colour channels, and (3) the green colour channel is analysed.

2.3. Structural behaviour

2.3.1. Development of crack widths

Fig. 1 shows the reinforcement configuration of the reinforced concrete beams tested in four-point bending. In all beams B500B ribbed reinforcement steel was used. The AAC beams were tested at different ages (e.g., 33 days, 69 days and 151 days) in our previous study [23]. One specimen was tested per age. For comparison, a reinforced NSC-52.5 beam, similar in design and test configuration, was tested at 33 days [47]. NSC-52.5 had an elastic compressive modulus of 34.36 GPa and a cubic compressive strength of 48.24 MPa at the age of 33 days. The tests were performed in displacement control with a loading rate of 0.01 mm/s. Linear variable differential transformers (LVDTs) were used to measure the mid-span deflection and elongation of the bottom surface over the constant bending moment region. 2D digital image correlation (DIC) was used to determine crack widths [48]. The accuracy and verification of the DIC data used has been previously confirmed [23,47]. Crack widths and their development throughout the test are monitored on a side face of the beam at approximately 2 mm from the bottom.

Analytical calculations were also used to predict the crack widths. These calculations were performed according to NEN-EN 1992-1-1:2011 [49] using the average material properties and disregarding the safety factors. The reinforcing steel is assumed to be bi-linear with a yielding strength of 550 MPa, an ultimate strength of 680 MPa and an elastic modulus (E_s) of 200 GPa.

AAC is known to exhibit significant drying shrinkage [18,19,21,26–28]. In reinforced concrete structures, shrinkage is restrained by the reinforcement, leading to internal stresses. Therefore, the combined action of restrained shrinkage deformation and external load is also considered for the S50 beams. Total shrinkage deformation

for S50 were previously measured on $100 \times 100 \times 400 \text{ mm}^3$ prisms exposed to 55% RH and 20°C after 28 days of fog curing. Shrinkage strain deformation (ϵ_{sh}) can lead to cracks if it exceeds the tensile strain capacity of concrete (ϵ_{ct}). The tensile strain capacity is obtained from notched $100 \times 100 \times 400 \text{ mm}^3$ prisms tested in three-point bending at different ages tested in our previous study [23]. If the tensile strain capacity (ϵ_{ct}) is exceeded by the shrinkage strain (ϵ_{sh}), the shrinkage moment (M_{sh}) is equal to the cracking moment (M_{cr}). Otherwise, shrinkage loads (M_{sh}) are determined by Eq. (1).

$$M_{sh}(t) = \frac{\epsilon_{sh}(t)}{\epsilon_{ct}(t)} M_{cr} \quad (1)$$

The cracking moment is determined by the moment of resistance (W) of a rectangular reinforced cross-section, and the mean tensile strength (f_{ctm}), see Eq. (2). The mean tensile strength over time (t) of the AACs is determined from the development of the splitting strength, $f_{ct,spi}$ per Eq. (3), in accordance with NEN-EN 1992-1-1:2011 [49]. For NSC-52.5, the tensile strength is determined from its compressive strength compressive strength, f_{ck} , per Eq. (4).

$$M_{cr}(t) = W f_{ctm}(t) \quad (2)$$

$$f_{ctm}(t) = 0.9 f_{ct,spi}(t) \quad (3)$$

$$f_{ctm}(t) = 0.3 f_{ck}^{\frac{2}{3}}(t) \quad (4)$$

As the shrinkage load is present prior to applying the short-term external load ($<1.5 \text{ h}$), the total acting moment on the beams is the sum of the moment caused by restrained shrinkage deformations and moment due to the externally applied load. The experimentally measured moments at cracking and at instances when the maximum crack width reaches 0.2 mm and 0.3 mm are compared to the analytically predicted values.

2.3.2. Development of bending stiffness

The measured elastic mid-span deflections are compared to analytical predictions. These analytical calculations usually assume isotropic behaviour of concrete in the linear elastic stage. Consequently, the elastic compressive modulus (E_c) and elastic tensile modulus (E_t) are assumed to be equal. This is a reasonable assumption given that the ratio between the elastic tensile modulus and the elastic compressive modulus for OPCCs is around 0.9 [50]. However, it is not clear if the same ratio and accompanying assumptions are valid for AACs. Therefore, besides the isotropic approach, a bi-modular approach as used in composite materials [51] is also investigated (Fig. 2).

The bi-modular approach assumes that a reinforced concrete beam is a composite material, composed of: (1) concrete in tension, (2) concrete in compression and (3) steel reinforcement. Furthermore, the following assumptions are made: deflections are small, plane sections remains plane and only in-plane bending occurs. The measured elastic compressive modulus is used for concrete in compression. Concrete in tension is characterized by the elastic tensile modulus, which has not been directly measured for the studied AACs. Therefore, it is determined from the mean tensile strength ($f_{ctm}(t)$) and mean tensile strain capacity ($\epsilon_{ct}(t)$). These properties are measured on notched $100 \times 100 \times 400 \text{ mm}^3$ prisms tested in three-point bending at different ages [23]. Eq. (5) can thus be used to determine the elastic tensile modulus.

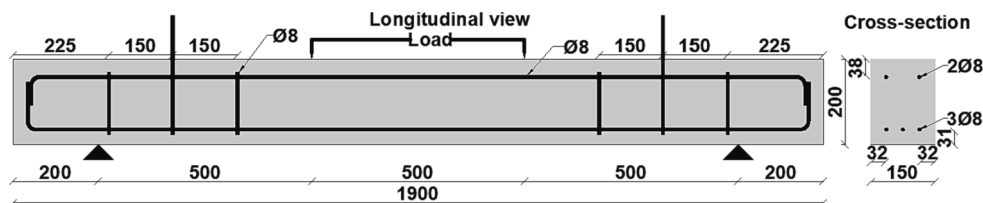


Fig. 1. Reinforcement configuration [23,47].

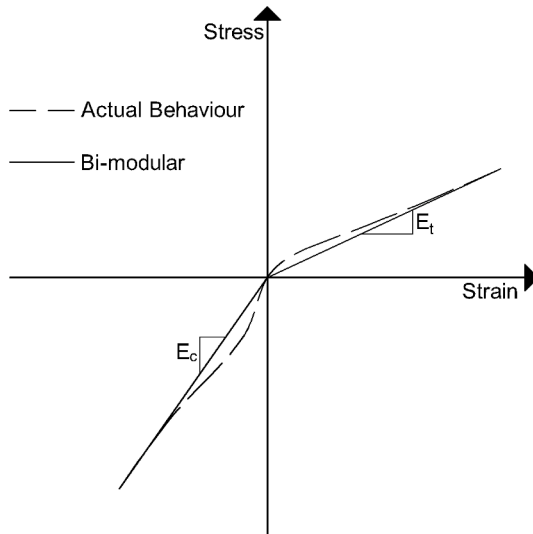


Fig. 2. Stress-strain curve for bi-modular materials adapted from [51]. Elastic tensile modulus and elastic compressive modulus are denoted by E_t and E_c , respectively.

$$E_t(t) = \frac{f_{ctm}(t)}{\epsilon_{ct}(t)} \quad (5)$$

The measured values of the mean elastic compressive modulus and elastic tensile modulus are sampled mean values assuming a normal distribution. Therefore, the propagated uncertainty of the ratio (standard deviation) is determined with a second order Taylor Expansion with Eq. (6) [52]

$$\text{Standard deviation} = \sqrt{\frac{\text{Var}(E_t)}{\bar{E}_c^2} + \text{Var}(E_c) \frac{\bar{E}_t^2}{\bar{E}_c^4} - 2\text{COV}\left(\frac{E_t}{E_c}\right) \frac{\bar{E}_t}{\bar{E}_c^3}} \quad (6)$$

where Var is the variance, COV is the covariance, and \bar{E}_c and \bar{E}_t are sample means. It is assumed that the elastic compressive modulus and elastic tensile modulus are correlated.

For NSC-52.5, the ratio between the tensile and compressive elastic modulus is assumed to be 0.86 [50]. The linear elastic mid-span deflection $w(t)$ at each testing age (t) is determined analytically following Eq. (7)

$$w(t) = \frac{1}{24} \left(3 - 4 \frac{a^2}{L^2} \right) \frac{FaL^2}{2EI_{composed}(t)} \quad (7)$$

where a is the length of the shear span, L is the span of the beam, F is the magnitude of the applied point-load (total load applied is $2F$) and $EI_{composed}(t)$ is the bending stiffness of the reinforced beam. The bending stiffness of a composite uncracked reinforced concrete beam is determined with Eq. (8)

$$\begin{aligned} EI_{composed} = & E_c \left(\frac{1}{12} bh_c^3 + bh_c \left(n.a. - \frac{1}{2} h_c \right)^2 \right) + \\ & E_t \left(\frac{1}{12} bh_t^3 + bh_t \left(n.a. - h_c - \frac{1}{2} h_t \right)^2 \right) + \\ & E_s \left(\frac{1}{4} (n_t + n_c) \pi R^2 + n_t \pi R^2 (h - n.a. - d_t)^2 + \right. \\ & \left. n_c \pi R^2 (n.a. - d_c)^2 \right) \end{aligned} \quad (8)$$

where h_t is the height of concrete under tension, h_c is the height of concrete under compression, b is the width of the beam, n_t and n_c are the

number of reinforcement bars in the tensile and compressive zones, respectively, R is the radius of the reinforcement bars, d_t and d_c are the distances from the centroid of the tensile and compressive reinforcement to the top of the beam, respectively and $n.a.$ is the distance from the top of the beam to the neutral axis. The position of the neutral axis ($n.a.$) is iteratively determined for each testing age, following force equilibrium. A first estimate of the position of the neutral axis ($n.a.$) is obtained by Eq. (9) [51]

$$n.a.(t) = \frac{\sqrt{E_t(t)}}{\sqrt{E_t(t)} + \sqrt{E_c(t)}} h \quad (9)$$

where h is the height of the beam. This would be the position of the neutral axis if concrete was unreinforced. These initial heights of the tensile zone (h_t) and compressive zone (h_c) are used to update the position of the neutral axis with Eq. (10).

$$n.a. = \frac{\frac{1}{2} bh_c^2 E_c + bh_t E_t (h_c + \frac{1}{2} h_t) + n_t \pi R^2 E_s (h - d_b) + n_c \pi R^2 E_s d_c}{bh_c E_c + bh_t E_t + (n_t + n_c) \pi R^2 E_s} \quad (10)$$

3. Results & discussion

3.1. Development of mechanical properties

3.1.1. Compressive strength

The development of the compressive strength over time is shown in Fig. 3a. This figure shows that S100 has a constant compressive strength over the monitoring period of 5 years. This observation is in line with earlier findings [12,17]. On the contrary, S50 shows a clear decrease in compressive strength (by 22%) between 2 and 5 years, while it was constant during the first 2 years. In our previous study [23] we have not observed this decrease, as the strength of these AACs was measured up to 2 years. The OPC concretes show a compressive strength increase of 74% and 15% for NSC-42.5 and HSC, respectively, from 28 days up to the tested age of 3.5 years (1304 days). This indicates that ongoing hydration of cement is dominant in these OPCCs [14], which is in line with earlier findings [7–13].

3.1.2. Tensile splitting strength

The evolution of the tensile splitting strength is shown in Fig. 3b. The splitting strengths, for both S100 and S50, show a decreasing trend up to their tested ages (around 5 years, i.e., 1981 days and 1983 days). In particular, S100 shows a significant decrease (by 21%) in the mean tensile splitting strength between 2 years and 5 years, while its tensile splitting strength was relatively constant for the first 2 years. Wardhono et al. [17] observed a similar trend for a GGBFS-based AAC. They, however, did not observe any decrease of strength over time in their FA-based AAC. On the contrary, the tensile splitting strength of S50 is continuously decreasing for all tested ages. Furthermore, the reduction in tensile strength of S50 is more significant compared to decrease of the compressive strength. A similar difference in the mechanical response between tension and compression has also been found in OPC-based concretes suffering from Alkali-Silica Reaction and has been attributed to the formation of weaker interfacial transition zones between cement paste and aggregates, for example due to microcracking [53]. The OPCCs show an increase in their tensile strengths until the tested age (3.5 years). A significant increase of 66% is found in the tensile splitting strength for NSC-42.5 between the age of 28 days and around 3.5 years, which is in line with published literature [10].

3.1.3. Elastic compressive modulus

The development of the elastic compressive modulus is shown in Fig. 3c. S50 shows a continuous decrease in its mean elastic modulus up to 30%, between 28 days and 5 years. On the other hand, S100 shows an initial 20% reduction of the mean elastic compressive modulus in the first 193 days. Beyond 193 days, the elastic modulus remains relatively

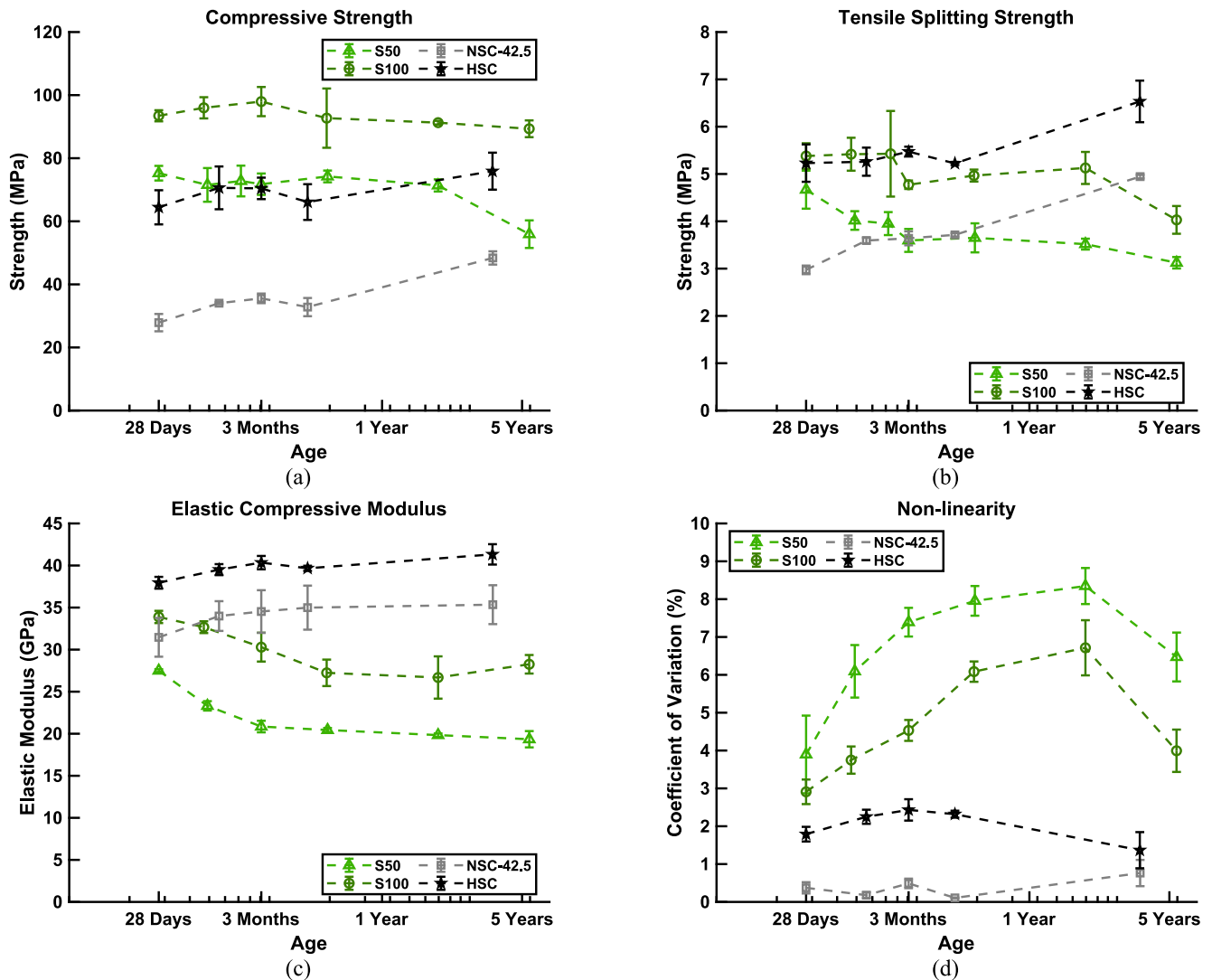


Fig. 3. Development of (a) compressive strength, (b) tensile splitting strength, (c) elastic compressive modulus and (d) non-linearity of stress–strain behaviour under compression for the AACs (S50, S100) and OPCCs (NSC-42.5, HSC) over time. The age is presented on a logarithmic scale. Results of AACs in the first 2 years by our previous study [23].

constant up to the tested age of 5 years. When it comes to OPCCs, the mean elastic compressive moduli of NSC-42.5 and HSC further increase between 28 days and 3.5 years. This increase is not in line with previously reported reductions of the elastic modulus for OPCCs under drying [54]. Hence, the effect of ongoing cement hydration in the studied OPCCs is dominant over the reduction in elastic modulus due to moisture loss and microcracking.

3.1.4. Non-linearity of the compressive Stress–strain behaviour

The development of the non-linearity in the compressive stress–strain response of the studied concretes is presented in Fig. 3d. Both AACs show more pronounced non-linearities compared to the OPCCs, as shown by their larger coefficient of variation at all tested ages. Furthermore, the coefficient of variation for S50 and S100 increases from 28 days up to an age of 2 years, while it remains relatively constant for the OPCCs. As the non-linearity has been linked with the presence of internal damage [44], the higher coefficient of variation for AACs indicates the presence of (micro)cracks. The increase of non-linearity over time indicates that the damage propagation is dominant in the AACs. Note that from the age of 2 to 5 years the non-linearity decreased. This could be attributed to a higher starting load used during the elastic compressive modulus test for the samples tested at an age of 5 years,

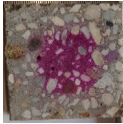
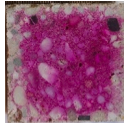
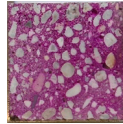
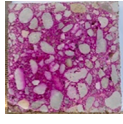
which was not used at 2 years. A minimum stress of 8% of the mean prism strength was maintained at later ages (5 years), in accordance with EN 12390–13 [40]. A minimum stress reduces the effect of settling of the sample, setup and measuring devices, and it prevents reopening of closed cracks. Despite this change in testing procedure, the results clearly indicate a decrease in the elastic compressive modulus for S50 and a significantly higher non-linearity for both AACs at the age of 5 years compared to the OPCCs.

3.1.5. Carbonation depth

The measured carbonation depths for different samples are summarized in Table 3. These results clearly show carbonation in the AACs. S50 shows a significant carbonation depth of 23.87 mm at an age of 5 years. This is in line with the previously reported carbonation depths and mechanisms of carbonation in AACs [25]. The observed decreases in mechanical properties for S50, especially for the compressive strength, can be attributed to carbonation [19]. On the contrary, S100 shows limited carbonation depth (4.24 mm) after 5 years. This is in agreement with findings from Nedeljković et al. [25] and can be explained by the dense pore structure, high Ca/Si ratio, and limited consumption of Na^+ ions from the pore solution of S100. Unlike AACs, the cement-rich OPCCs (NSC-42.5 and HSC) show no carbonation, as expected for

Table 3

Carbonation depth for the investigated materials at an age of 3.5 and 5 years. The standard deviation is reported in brackets.

	S50	S100	NSC-42.5	HSC
Age (days)	1989	1987	1304	1299
Sample 1 (mm)	25.22	4.73	0	0
Sample 2 (mm)	23.59	4.87	0	0
Sample 3 (mm)	22.81	3.11	0	0
Mean (mm)	23.87 (± 1.23)	4.24 (± 0.98)	0	0
Concrete cross section ($100 \times 100 \text{ mm}^2$)				

OPCCs [25,55].

3.1.6. Microscopic analysis

The microscopic results are presented in Fig. 4. The dashed lines indicate the centre of the original samples (i.e., areas which were not directly exposed to drying and carbonation), as the samples are cut from larger elements ($100 \times 100 \text{ mm}^2$). It can be observed that there is more epoxy penetration close to the exterior surfaces of AACs compared to the cores. This difference in penetration over the cross section is not observed for the OPCCs. To quantify the difference in epoxy impregnation between the surface layer and the core of the concretes, the average grey-scale value (on a scale of 0 to 255) is determined at 3 representative areas in the exterior layer and 3 representative areas in

the core (Table 4). A square of $3 \times 3 \text{ mm}^2$ containing only small aggregates and no large voids is considered to be a representative area. These results show that S100 has the largest difference in greyscale-

Table 4

Variation of grey scale value from exterior to core of the specimens. Grey scale values are on a scale of 0 to 255. Standard deviations are mentioned in brackets.

Label	Mean Exterior	Mean Core	Difference
NSC-42.5	69.72 (± 3.94)	65.49 (± 6.11)	4.23
HSC	38.24 (± 0.93)	35.84 (± 13.78)	2.40
S50	61.37 (± 6.17)	17.67 (± 3.36)	43.70
S100	98.57 (± 8.79)	8.55 (± 5.85)	90.03

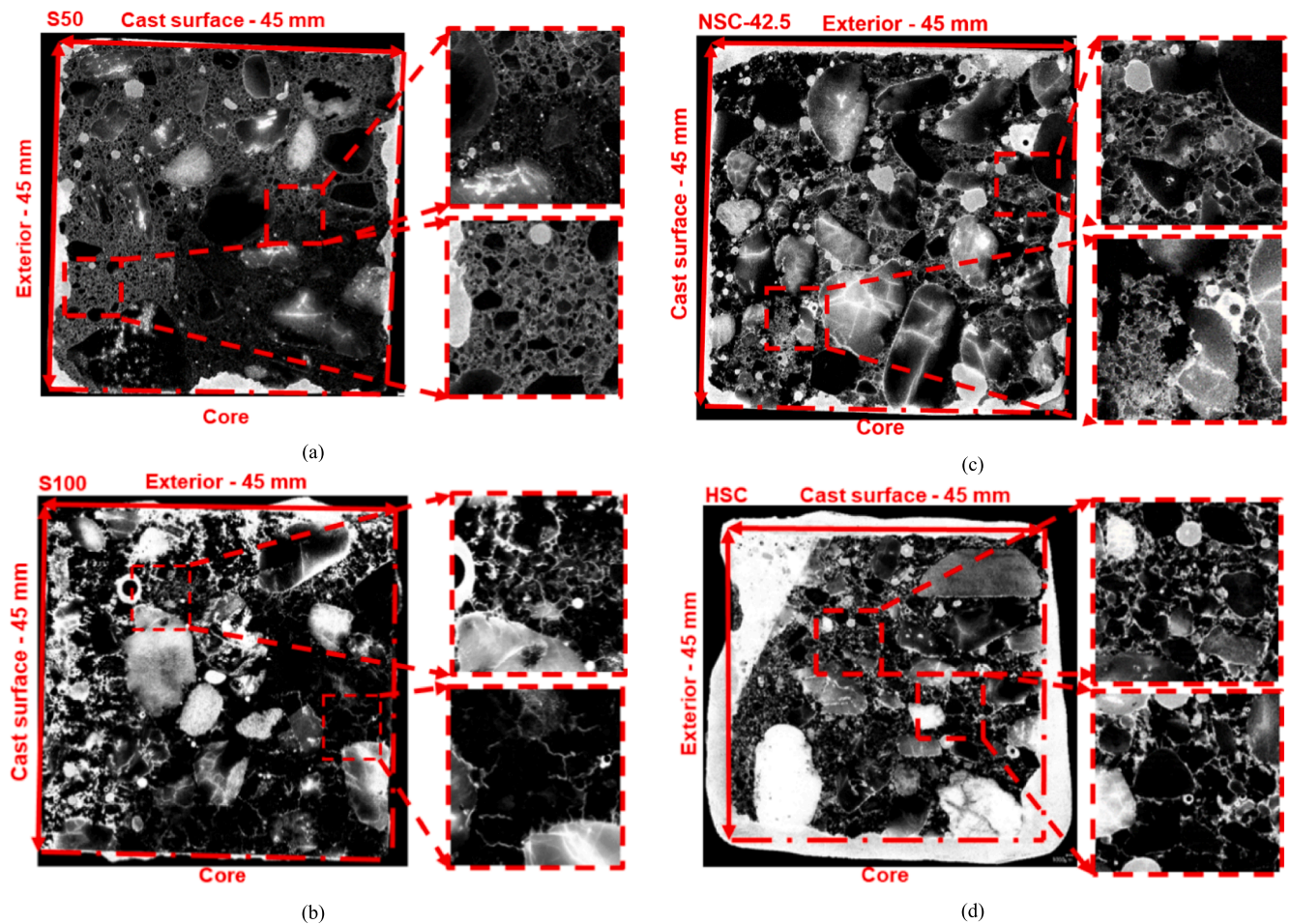


Fig. 4. Microscopic analysis of epoxy impregnated $45 \times 45 \text{ mm}^2$ samples under UV light, shown by 8-bit green colour channel images for (a) S50, (b) S100, (c) NSC-42.5 and (d) HSC with zoomed sections to indicate the affected/damaged surface area. (For interpretation of the references to colour in this figure legend, the reader is referred to the web version of this article.)

value between its exterior layer and core. S50 also has a significant difference in its grey-scale values, whereas no differences are found over the cross section of the OPCCs.

The thickness of porous surface layers is larger for S50 compared to S100, which is in line with the measured carbonation depths. While epoxy penetrates pores and (micro)cracks, the used level of detail in the microscopic analysis is insufficient to distinguish between the two. However, microcracks could be observed in S50 and S100 and not in the OPCCs. Especially, S100 showed significant microcracking close to its exterior surface. Microcracks were also observed on the surface of both AACs by an optical microscope. Similar as for the epoxy impregnated images, S100 showed significant microcracking, while only a few microcracks are observed for S50. This is in agreement with the observation of microcracks on the surface for GGBFS-based AACs by Nedeljković et al. [15]. These findings indicate that decreases in the mechanical properties of AACs are not temporary, as previously hypothesized. As the carbonation depth was limited in S100, a different mechanism must be responsible for the microcracking and the observed decrease in mechanical properties. A possible reason is the chemical change in the microstructure under drying, since chemically bound water is easily removed from C-A-S-H gels under drying at ambient temperatures [29]. The removal of this chemically bound water causes desiccation of C-A-S-H gels [29]. No notable chemical changes were reported in FA/GGBFS-based binders because they had most of their water physically bound [29]. Another reason for the more significant cracking of S100 could be drying shrinkage, because GGBFS-based AACs have finer pore structures compared to binary AACs [25,27].

3.2. Structural behaviour

3.2.1. Crack width development over time

As the decreases in mechanical properties are not temporary, it is vital to understand the significance of these decreases on the development of crack widths in reinforced concrete beams tested at later ages. The measured crack widths are compared with analytical predictions. Also, the effect of shrinkage is included in the analytical model. Fig. 5 presents the development of the shrinkage and the tensile strain capacity of S50 over time. These results show that the mean strain capacity of S50 is not exceeded by shrinkage strains for all tested ages. Hence, S50 did not crack due to shrinkage. This is in line with the findings of Li et al. [56], who did not observe shrinkage cracking in AAC if exposure started after a curing period of 28 days.

Fig. 6a shows the experimentally measured bending moment – deflection curves and maximum crack width – deflection curves for all

the studied beams. These results show that the AACs have a lower tension stiffening effect than NSC-52.5 at the age of 34 days. The tension stiffening effect decreases for both AACs over time. Fig. 6b shows the cracking bending moments for the studied beams. While comparable cracking bending moments are observed for AACs and NSC-52.5 at the age of 33 days, both AACs show clear decreases over time. For example, S50 shows a 12% decrease in its cracking bending moment from 33 days to 69 days. This decrease could be attributed to the development of mechanical properties, as the analytical prediction reflects this decrease with a maximum deviation of 2%. On the other hand, the decreases for S100 could not be accurately predicted by its mechanical properties as the prediction overestimated the cracking bending moment by 14%.

The bending moments at which a maximum crack width of 0.2 mm or 0.3 mm is reached are presented in Fig. 6b. These bending moments are similar for S50 and NSC-52.5 at the age of 34 days. However, the bending moment at which 0.3 mm crack width is reached in S100 is 17% lower compared to that of NSC-52.5 and S50 at the age of 34 days. Larger crack widths for GGBFS-based AACs at the age of 28 days were also observed by Du et al. [35]. Furthermore, larger crack widths are observed for both AACs tested at later ages. For example, the bending moment at which a maximum crack width of 0.2 mm is obtained decreases (by 22%) for S100 from 34 days to 70 days. Similarly for S50, the load at which the crack of 0.2 mm is reached seems to reduce from 34 days to 151 days. Although there is no statistically representative number of samples, the general trends can still be observed and confirmed by analytical calculations.

Without accounting for shrinkage, the bending moments at which the crack widths of 0.2 mm and 0.3 mm are reached could be reasonably well predicted for NSC-52.5 at an age of 34 days. On the contrary, the loads at which a crack width criterion is reached was always overestimated for the AACs if shrinkage was not accounted for. For example, the load at which the maximum crack width reached 0.2 mm for S100 was overestimated by 64% at an age of 70 days. If shrinkage is accounted for in S50, the prediction of crack widths is almost always conservative. Note, in this study only the total shrinkage increase after 28 days of moist curing is accounted for and, therefore, the effect of autogenous shrinkage during the curing period is neglected. Although autogenous shrinkage has been reported to be significant for AACs [15], AACs also exhibit significant creep [12,19,21,26]. Creep deformation in total autogenous shrinkage is significant compared to the elastic deformation and only the elastic deformation leads to stresses. As a result, the cracking tendency of AACs, following the classification defined by ASTM C1581 [57], under restrained autogenous shrinkage is moderate-low [22]. Creep effects in drying shrinkage measurements are not considered, which leads to the overestimation of the internal stresses caused by restrained drying shrinkage deformation. Including creep effects (i.e., estimating the elastic component of drying shrinkage) in the analysis might improve the prediction of long-term crack widths and is recommended to be included in future studies. Furthermore, the current analytical crack width prediction model assumes a constant rebar-concrete bond over time, whereas this assumption might not be valid if internal (micro)cracks are formed. The bond behaviour has not been monitored over time and should thus be included in future works.

A decrease in the bending moments at which the crack width limits are reached for S50 is observed at an age of 69 days compared to 151 days. This could not be predicted by the development of mechanical properties nor by accounting for shrinkage. The cracking pattern was similar to the AAC beams tested at 33 days and 151 days, while the ultimate capacity was reduced by 13% [23]. As it is uncertain what the statistical relevance is of this deviation, future studies should address the repeatability of these structural tests.

3.2.2. Bending stiffness development over time

The analytically predicted ratios between the tensile elastic moduli and elastic compressive moduli for the studied AACs are presented in Fig. 7a. Although their standard deviations are quite significant, the

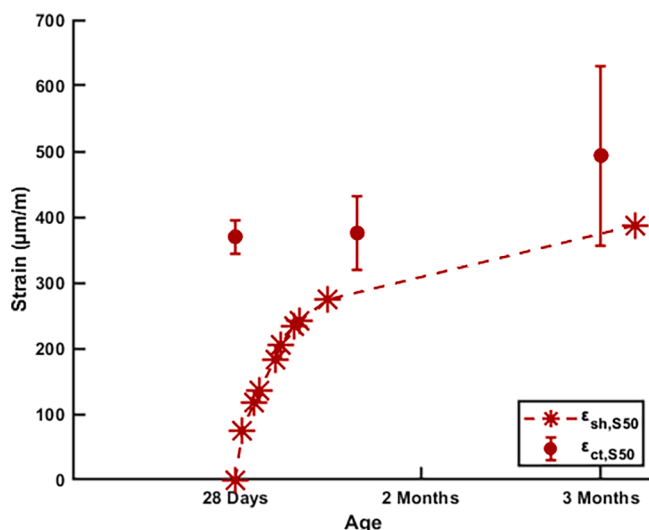


Fig. 5. Total shrinkage (ϵ_{sh}) and strain capacity (ϵ_{ct}) of S50 over time.

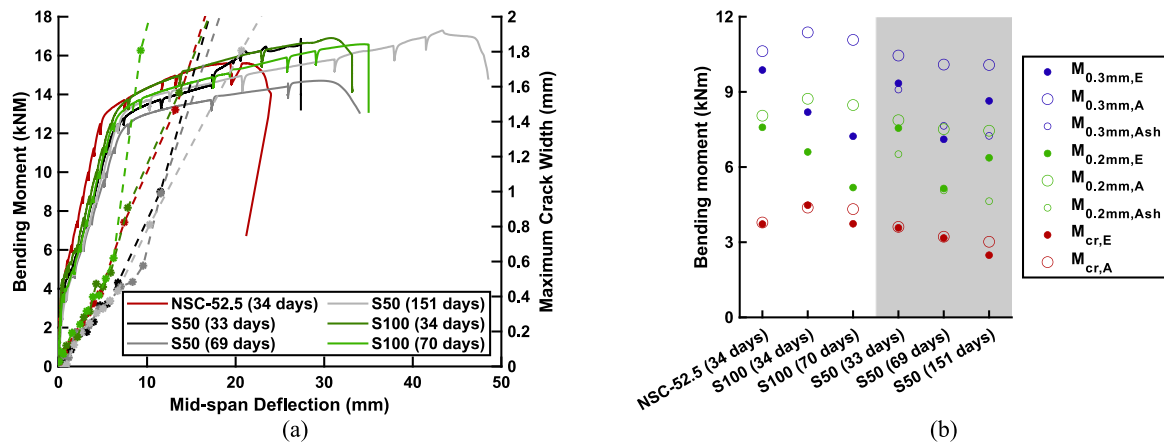


Fig. 6. (a) Experimentally obtained bending moment – deflection curves (solid lines) and maximum crack width – deflection curves (dashed lines) for the studied beams. Results by Prinse et al. [23]. (b) Comparison of experimentally observed (E) bending moments with analytical calculations with (A_{sh}) and without (A) shrinkage for the reinforced concrete beams tested at different ages. The age of the beams is mentioned in brackets. $M_{0.3mm}$ = bending moment at 0.3 mm crack width. $M_{0.2mm}$ = bending moment at 0.2 mm crack width. M_{cr} = cracking moment.

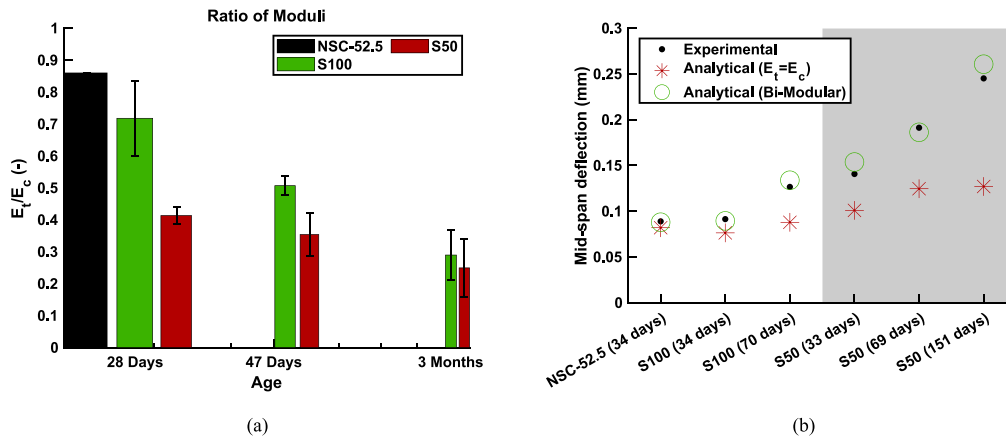


Fig. 7. (a) Ratio of the elastic tensile modulus and the elastic compression modulus for AACs and NSC-52.5 over time. The age is presented on a logarithmic scale. (b) Comparison of elastic mid-span deflections obtained with the conventional analytical approach, bi-modular approach and as observed in experiments. The elastic mid-span deflections are determined from 5 to 10 kN of load for the tested beams at different ages. The testing ages of the beams are mentioned in brackets.

ratio between the moduli shows that the elastic tensile modulus is lower for both AACs compared to that of NSC-52.5, at an age of 34 days. For example, the ratio of the tensile to compressive modulus for S50 at 28 days is 0.41. The ratio of moduli decreases over time for both AACs. For example, at the age of 91 days, both S50 and S100 show an elastic tensile modulus of 32% of the elastic compressive modulus. An explanation for the significant decrease in elastic tensile modulus over time for S100 might be the formation of shrinkage cracks and drying-induced chemical changes in the microstructure. As (drying) shrinkage was not measured for S100, it is recommended to include shrinkage measurements in future studies. The elastic tensile moduli and the ratios are indirectly determined, and are significantly lower compared to experimentally reported values for conventional concrete by Tipka et al. [50]. To verify the obtained results and the adopted bi-modular approach, the tensile elastic modulus of AACs should be measured in the future.

The elastic mid-span deflections for reinforced concrete beams tested at later ages are shown in Fig. 7b. Deflection increments in the load range from 5 to 10 kN are analysed, to eliminate settling effects of the beams. The results show that deflections for S50 are already 53–58% larger compared to those for NSC-52.5 and S100 at the age of 34 days. This could be attributed to the lower elastic moduli of S50 in tension (53%) and compression (81%) compared to NSC-52.5 at the age of 28 days. The lower elastic compressive modulus for AACs, compared to

OPCCs, is in agreement with earlier findings [16,22,35,58] and might be related to the intrinsically lower elastic modulus of the N-A-S-H and C-A-S-H gels in AACs compared to C-S-H gels in OPCCs [59].

Furthermore, the elastic mid-span deflection increases for the AACs over time. In other words, their bending stiffness decreases over time. The bending stiffness of S100 decreases by 38% from 34 days to 70 days. Interestingly, a similar decrease is observed for S50 from 33 days to 69 days, whereas the two AACs have a different governing degradation mechanism and different decreases in elastic moduli over time. For example, the decrease in elastic compressive modulus is more significant for S50, while S100 shows a more significant decrease in its tensile elastic modulus from 28 days to 91 days. The decrease in bending stiffnesses for the studied AACs over time could, in addition to creep, be a reason for significant deflection increase under sustained load in reinforced FA/GGBFS-based AAC beams observed by Un et al. [18]. More research is needed to distinguish between the contribution of creep and reduction of bending stiffness of AACs to develop long-term deflection prediction models.

Comparison of these experimentally obtained deflections with conventional analytical predictions, where it is assumed that the elastic modulus in tension and compression are equal ($E_t = E_c$), shows that the deflections are underestimated for the AACs at all tested ages (Fig. 6b). This underestimation of mid-span deflections increases for beams tested

at later ages. For example, a deflection increase of only 15% is analytically predicted for S100 from 34 days to 70 days, while an increase of 38% is experimentally observed. If bi-modularity is assumed ($E_t < E_c$), the accuracy of the mid-span deflection prediction improves significantly.

4. Conclusions

A series of tests were performed to investigate the long-term mechanical properties of two OPC based concretes and two AACs (one GGBFS-based and one FA/GGBFS-based AAC) up to the age of 3.5 and 5 years, respectively. Additional analyses were performed to reveal underlying mechanisms. With the gained insights, crack widths and bending stiffnesses in reinforced concrete beams tested at different ages were analysed and the applicability of analytical models used for conventional concrete were evaluated. A bi-modular approach is proposed for the prediction of bending stiffness of reinforced concrete beams. The following conclusions can be drawn from this study:

- Earlier reported decreases in mechanical properties of two AACs exposed to 55% RH and 20 °C are unlikely to be temporary. The tensile splitting strength and elastic compressive modulus continued to decrease for the studied FA/GGBFS-based AAC up to the monitored age of 5 years, while the studied GGBFS-based AAC showed a 22% decrease in tensile splitting strength from 2 to 5 years. Although the compressive strength was stable for the FA/GGBFS-based AAC up to the age of 2 years, it reduced (by 22%) between 2 and 5 years. On the contrary, all studied mechanical properties increased for the OPC concretes tested up to the age of 3.5 years.
- Unlike the OPCCs, the AACs showed significant increases in the non-linearity of the stress-strain behaviour under compression. Different underlying mechanisms are found for the two AAC mixtures. Significant carbonation (23.87 mm) was observed for FA/GGBFS-based AAC at the age of 5 years. Although the carbonation depth was limited (4.24 mm) for the GGBFS-based AAC, microcracks were observed under the microscope. These microcracks are probably a result of chemical changes in the microstructure under drying and drying shrinkage. The OPC concretes did not show carbonation nor microcracking at the age of 3.5 years.
- Reinforced GGBFS-based AAC beams showed larger crack widths than OPCC and FA/GGBFS-based AAC beams at the age of 34 days. Furthermore, larger crack widths were observed if GGBFS-based and FA/GGBFS-based AACs were tested at later ages. These increases could not be analytically predicted by only accounting for the decreases in their mechanical properties over time. If the increase in total shrinkage after 28 days of fog-curing was accounted for in the analytical prediction of crack widths over time, the predicted bending moments at which a maximum crack width of 0.2 mm and 0.3 mm is reached became conservative.
- The FA/GGBFS-based AAC showed a lower bending stiffness than the GGBFS-based AAC and the OPCC at the age of 33 days. This can be attributed to the lower elastic compressive modulus and lower elastic tensile modulus for FA/GGBFS-based AAC at the age of 28 days and can be related to the intrinsically lower Young's modulus of gel-paste for the binary AAC compared to GGBFS-based AAC and OPCC.
- The bending stiffness of the studied AACs decreased over time. Although the AACs had a different governing degradation mechanism, similar decreases in bending stiffness were observed over time. Reductions in bending stiffness of the AACs over time were significantly underestimated if they were assumed to behave isotropic. If AACs were assumed to be bi-modular, predictions of their bending stiffness were more accurate.

It is important to note that the current study focuses on two specific AACs and compares them with two OPC-based concretes under specific exposure conditions (55% RH and 20 °C). Therefore, different results

might be found for different binders in AACs or under different exposure conditions. Future studies will focus on different binder compositions in AACs. To obtain a more realistic estimate of the development of internal stresses and improve the prediction of crack widths in AACs over time, future studies should determine the contribution of creep to the apparent shrinkage under drying. Lastly, direct tensile tests are foreseen for AACs to verify the proposed bi-modular approach.

CRediT authorship contribution statement

H.J. Bezemer: Conceptualization, Investigation, Formal analysis, Writing – original draft. **N. Awasthy:** Investigation. **M. Luković:** Conceptualization, Supervision, Writing – review & editing.

Declaration of Competing Interest

The authors declare that they have no known competing financial interests or personal relationships that could have appeared to influence the work reported in this paper.

Data availability

Data will be made available on request.

Acknowledgements

This work is supported by the project AshCycle, which is funded by the European Union (Grant number 101058162). The authors would like to express their gratitude for the obtained lab support.

References

- [1] P.-C. Aitcin, Cements of yesterday and today Concrete of tomorrow, *Cem. Concr. Res.* 30 (2000) 1349–1359.
- [2] D.N. Huntzinger, T.D. Eatmon, A life-cycle assessment of Portland cement manufacturing: comparing the traditional process with alternative technologies, *J. Clean. Prod.* 17 (7) (2009) 668–675.
- [3] S.A. Miller, A. Horvath, P.J.M. Monteiro, Readily implementable techniques can cut annual CO₂-emissions from the production of concrete by over 20%, *Environ. Res. Lett.* 11 (7) (2016).
- [4] K.L. Scrivener, R.J. Kirkpatrick, Innovation in use and research on cementitious material, *Cem. Concr. Res.* 38 (2) (2008) 128–136.
- [5] IEA, Technology Roadmap - Low-Carbon Transition in the Cement Industry, IEA, Paris, 2018.
- [6] K.-H. Yang, J.-K. Song, K.-I. Song, Assessment of CO₂ reduction of alkali-activated concrete, *J. Clean. Prod.* 39 (2013) 265–272.
- [7] V.M. Malhotra, M. Zhang, P.H. Read, J. Ryell, Long-Term Mechanical Properties and Durability Characteristics of High-Strength/High-Performance Concrete Incorporating Supplementary Cementing Materials under Outdoor Exposure Conditions, *ACI Mater. J.* 97 (2000) 518–525.
- [8] S. Khatibmasjedi, F. De Caso, A. Nanni, SEACON: Redefining Sustainable Concrete. 4th International Conference in Sustainable Construction Materials and Technologies Las Vegas, 2016.
- [9] S.-Y. Jia, M.-H. Liu, B. Han, H.-B. Xie, An elastic modulus developing model of fly ash concrete under sustained load, *KSCE J. Civ. Eng.* 22 (7) (2017) 2417–2424.
- [10] A. Gholampour, T. Ozbakkaloglu, Time-dependent and long-term mechanical properties of concretes incorporating different grades of coarse recycled concrete aggregates, *Eng. Struct.* 157 (2018) 224–234.
- [11] R. Sarkhosh, Shear resistance of reinforced concrete beams without shear reinforcement under sustained loading [doctoral dissertation], Technical University of Delft, Delft, 2014.
- [12] J. Ma, F. Dehn, Shrinkage and creep behavior of an alkali-activated slag concrete, *Struct. Concr.* 18 (5) (2017) 801–810.
- [13] S.A. Bernal, R. Mejía de Gutiérrez, A.L. Pedraza, J.L. Provis, E.D. Rodriguez, S. Delvasto, Effect of binder content on the performance of alkali-activated slag concretes, *Cem. Concr. Res.* 41 (1) (2011) 1–8.
- [14] H.W. Reinhardt, Factors affecting the tensile properties of concrete, in: J. Weerheijm (Ed.), *Understanding the Tensile Properties of Concrete*, Woodhead Publishing, 2013, pp. 19–51, <https://doi.org/10.1533/9780857097538.1.19>.
- [15] M. Nedeljkovic, Z. Li, G. Ye, Setting, strength, and autogenous shrinkage of alkali-activated fly ash and slag pastes: effect of slag content, *Materials* 11 (11) (2018).
- [16] S. Fernando, C. Gunasekara, D.W. Law, M.C.M. Nasvi, S. Setunge, R. Dissanayake, M.G.M.U. Ismail, Long-term mechanical properties of blended fly ash—rice husk ash alkali-activated concrete, *ACI Mater. J.* 119 (5) (2022).

- [17] A. Wardhono, C. Gunasekara, D.W. Law, S. Setunge, Comparison of long term performance between alkali activated slag and fly ash geopolymer concretes, *Constr. Build. Mater.* 143 (2017) 272–279.
- [18] C.H. Un, J.G. Sanjayan, R. San Nicolas, J.S.J. van Deventer, Predictions of long-term deflection of geopolymer concrete beams, *Constr. Build. Mater.* 94 (2015) 10–19.
- [19] A.M. Humad, J.L. Provis, K. Habermehl-Cwirzen, M. Rajczakowska, A. Cwirzen, Creep and long-term properties of alkali-activated swedish-slag concrete, *J. Mater. Civ. Eng.* 33 (2) (2021).
- [20] F.G. Collins, J.G. Sanjayan, Microcracking and strength development of alkali activated slag concrete, *Cem. Concr. Compos.* 23 (2001) 345–352.
- [21] F.G. Collins, J.G. Sanjayan, Workability and mechanical properties of alkali activated slag concrete, *Cem. Concr. Res.* 29 (1999) 455–458.
- [22] Z. Li, S. Zhang, X. Liang, G. Ye, Cracking potential of alkali-activated slag and fly ash concrete subjected to restrained autogenous shrinkage, *Cem. Concr. Compos.* 114 (2020).
- [23] S. Prinsse, D.A. Hordijk, G. Ye, P. Legendijk, M. Luković, Time-dependent material properties and reinforced beams behavior of two alkali-activated types of concrete, *Struct. Concr.* 21 (2) (2019) 642–658.
- [24] S.A. Bernal, R. San Nicolas, J.L. Provis, R. Mejía de Gutiérrez, J.S.J. van Deventer, Natural carbonation of aged alkali-activated slag concretes, *Mater. Struct.* 47 (4) (2013) 693–707.
- [25] M. Nedeljkovic, Carbonation mechanism of alkali-activated fly ash and slag materials in view of long-term performance predictions [doctoral dissertation], Technical University of Delft, Delft, 2019.
- [26] M. Hojati, F. Rajabipour, A. Radlińska, Drying shrinkage of alkali-activated cements: effect of humidity and curing temperature, *Mater. Struct.* 52 (6) (2019).
- [27] D. Huang, P. Chen, H. Peng, Y. Yang, Q. Yuan, M. Su, A review and comparison study on drying shrinkage prediction between alkali-activated fly ash/slag and ordinary Portland cement, *Constr. Build. Mater.* 305 (2021).
- [28] Z. Li, B. Delsaute, T. Lu, A. Kostuchenko, S. Staquet, G. Ye, A comparative study on the mechanical properties, autogenous shrinkage and cracking proneness of alkali-activated concrete and ordinary Portland cement concrete, *Constr. Build. Mater.* 292 (2021).
- [29] I. Ismail, S.A. Bernal, J.L. Provis, S. Hamdan, J.S.J. van Deventer, Drying-induced changes in the structure of alkali-activated pastes, *J. Mater. Sci.* 48 (9) (2013) 3566–3577.
- [30] M. Albitar, M.S. Mohamed Ali, P. Visintin, Evaluation of tension-stiffening, crack spacing and crack width of geopolymer concretes, *Constr. Build. Mater.* 160 (2018) 408–414.
- [31] A. Shah, C.B. Shah, Comparison of load-displacement relationship and crack development mechanism in reinforced geopolymer concrete beams with that of regular reinforced concrete beams. International Conference on Advances in Construction Materials and Systems, Chennai, 2017.
- [32] Z. Qian, E.O.L. Lantsoght, M. Lukovic, A critical review on structural behavior of alkali-activated concrete beams, in: 14th fib International PhD Symposium in Civil Engineering, Rome, 2022, pp. 273–280.
- [33] J.R. Yost, A. Radlińska, S. Ernst, M. Salera, N.J. Martignetti, Structural behavior of alkali activated fly ash concrete. Part 2: structural testing and experimental findings, *Mater. Struct.* 46 (3) (2012) 449–462.
- [34] D.M.J. Sumajouw, D. Hardjito, S.E. Wallah, B.V. Rangan, Fly ash-based geopolymer concrete: study of slender reinforced columns, *J. Mater. Sci.* 42 (9) (2006) 3124–3130.
- [35] Y. Du, J. Wang, C. Shi, H.-J. Hwang, N. Li, Flexural behavior of alkali-activated slag-based concrete beams, *Eng. Struct.* 229 (2021).
- [36] C. Wu, H.-J. Hwang, C. Shi, N. Li, Y. Du, Shear tests on reinforced slag-based geopolymer concrete beams with transverse reinforcement, *Eng. Struct.* 219 (2020).
- [37] M. Nedeljković, B. Ghiassi, S. van der Laan, Z. Li, G. Ye, Effect of curing conditions on the pore solution and carbonation resistance of alkali-activated fly ash and slag pastes, *Cem. Concr. Res.* 116 (2019) 146–158.
- [38] Nen, Testing hardened concrete - Part 3: Compressive strength of test specimens, NEN-EN 12390-3: 2019, European Committee for Standardization, Brussels, 2019.
- [39] Nen, Testing hardened concrete - Part 6: Tensile splitting strength of test specimens NEN-EN 12390-6: 2009, European Committee for Standardization, Brussels, 2009.
- [40] Nen, Testing hardened concrete - Part 13: Determination of secant modulus of elasticity in compression, NEN-EN 12390-13: 2021, European Committee for Standardization, Brussels, 2021.
- [41] A.M. Neville, J.J. Brooks, *Concrete Technology*, 2 ed., Pearson Education Ltd., London, 2010.
- [42] A. Talaat, A. Emad, A. Tarek, M. Masboub, A. Essam, M. Kohail, Factors affecting the results of concrete compression testing: A review, *Ain Shams Eng. J.* 12 (1) (2021) 205–221.
- [43] C.K. Kankam, B.K. Meisuh, G. Sossou, T.K. Buabin, Stress-strain characteristics of concrete containing quarry rock dust as partial replacement of sand, *Case Stud. Constr. Mater.* 7 (2017) 66–72.
- [44] C. t.m., w. p, w. j.g.m., Development of a non-destructive test to quantify damage in deteriorated concrete, *Mag. Concr. Res.* 45 (1993) 247–256.
- [45] Nen, Products and systems for the protection and repair of concrete structures - Test methods - Determination of resistance to carbonation NEN-EN 13295: 2004, European Committee for Standardization, Brussels, 2004.
- [46] T. Ferreira, W. Rasband, *ImageJ User Guide*, ImageJ/Fiji (2012) 132–146.
- [47] M. Lukovic, D. Hordijk, Z. Huang, E. Schlangen, Strain Hardening cementitious composite (SHCC) for crack width control in reinforced concrete beams, *Heron* 64 (2019) 189–206.
- [48] G. Ruocci, C. Rospars, G. Moreau, P. Bisch, S. Erlicher, A. Delaplace, J.M. Henault, Digital Image Correlation and Noise-filtering Approach for the Cracking Assessment of Massive Reinforced Concrete Structures, *Strain* 52 (6) (2016) 503–521.
- [49] NEN, Eurocode 2: Design of concrete structures - Part 1-1: General rules and rules for buildings. NEN-EN 1992-1-1+C2: 2011 (NL), European Committee for Standardization, Brussels, 2011.
- [50] M. Tipka, J. Vašková, Modulus of elasticity in tension for concrete and fibre reinforced concrete, *Solid State Phenom.* 259 (2017) 35–40.
- [51] R.M. Jones, Apparent Flexural Modulus and Strength of multimodulus materials, *Composite Materials* 10 (1976).
- [52] H. Benaroya, S.M. Han, *Probability Models in Engineering and Science*, 1 ed., Taylor & Francis Group, 2005.
- [53] R. Esposito, C. Anaç, M.A.N. Hendriks, O. Çopuroğlu, Influence of the Alkali-Silica Reaction on the Mechanical Degradation of Concrete, *J. Mater. Civ. Eng.* 28 (6) (2016).
- [54] I. Maruyama, H. Sasano, Y. Nishioka, G. Igarashi, Strength and Young's modulus change in concrete due to long-term drying and heating up to 90°C, *Cem. Concr. Res.* 66 (2014) 48–63.
- [55] O. Çopuroğlu, E. Schlangen, Modeling of frost salt scaling, *Cem. Concr. Res.* 38 (1) (2008) 27–39.
- [56] Z. Li, J. Liu, G. Ye, Drying shrinkage of alkali-activated slag and fly ash concrete a comparative study with ordinary portland cement concrete, *Heron* 64 (2019) 149–163.
- [57] Astm, Standard Test Method for Determining Age at Cracking and Induced Tensile Stress Characteristics of Mortar and Concrete under Restrained Shrinkage, ASTM C1581 (2009) 1–7.
- [58] J.R. Yost, A. Radlińska, S. Ernst, M. Salera, Structural behavior of alkali activated fly ash concrete. Part 1: mixture design, material properties and sample fabrication, *Mater. Struct.* 46 (3) (2012) 435–447.
- [59] Y. Ding, J.-G. Dai, C.-J. Shi, Mechanical properties of alkali-activated concrete: A state-of-the-art review, *Constr. Build. Mater.* 127 (2016) 68–79.